Implementation of a Particle Resuspension Model in a CFD Code: Application to an Air Ingress Scenario in a Vacuum Toroidal Vessel

Thomas Gelain, Laurent Ricciardi, Francois Gensdarmes

Proceedings of ICONE28-POWER2020
28th International Conference on Nuclear Engineering
August 2 - 6, 2020, Anaheim, USA

ICONE28-POWER2020-16139

IMPLEMENTATION OF A PARTICLE RESUSPENSION MODEL IN A CFD CODE – APPLICATION TO AN AIR INGRESS SCENARIO IN A VACUUM TOROIDAL VESSEL

Thomas GELAIN
Institut de Radioprotection et de Sûreté Nucléaire (IRSN)
PSN-RES, SCA
Gif-sur-Yvette, 91192, France

Laurent RICCIARDI
Institut de Radioprotection et de Sûreté Nucléaire (IRSN)
PSN-RES, SCA
Gif-sur-Yvette, 91192, France

François GENSDARMES
Institut de Radioprotection et de Sûreté Nucléaire (IRSN)
PSN-RES, SCA
Gif-sur-Yvette, 91192, France

Keywords: aerosol, resuspension, CFD, tokamak, LOVA

ABSTRACT

During a loss of vacuum accident (LOVA), dust particles that will be present in the future tokamak ITER are likely to be resuspended, inducing a risk for explosion and airborne contamination. Evaluating the particle resuspension/deposition and resulting airborne concentration in case of a LOVA is therefore a major issue and it can be investigated by using a CFD code. To this end, this article presents the implementation of a resuspension model in a CFD code (ANSYS CFX) and its application to an air ingress in a vacuum toroidal vessel with a volume comparable to ITER one.

In the first part of the article, the Rock'n Roll model and its operational version with the Biasi's correlation is presented.

The second part of the article will be devoted to the implementation of the Rock'n'Roll model in ANSYS CFX for constant friction velocities and its adaptation to non-constant friction velocities.

Finally, the paper presents the simulations obtained on the particle resuspension for an air ingress scenario in a large vacuum vessel. This case is particularly interesting and non-intuitive because as the initial pressure is reduced, the particle behavior is different from that at atmospheric pressure. Further, a competition between airflow forces and gravitational force occurs, due to the low pressure environment, potentially restricting the resuspension, and the pressure influence also has to be taken into account in the particle transport and deposition (Nerisson, 2011).

Three particle diameters were studied allowing to show the evolution of the resuspension with this parameter and to calculate dust resuspension rates and airborne fractions during the air ingress.

1. INTRODUCTION

As part of the construction of ITER, it is important to develop knowledge that ensures the highest level of safety in the nuclear facility (Van Dorsselaere *et al*., 2012). To assess the safety of nuclear facilities and the relevance of associated radiation protection measures, a key step consists in determining source terms of contamination during normal operation and for various accident scenarios. Since it concerns potential contamination in aerosol form, source terms are calculated by using resuspension coefficients to link the quantity of aerosol formed to the quantity of matter that may potentially be dispersed, depending on the scenario.

In ITER's normal operating conditions, several hundred kilograms of particles containing beryllium (Be) and tungsten (W) will be produced following erosion of the walls of the vacuum vessel (blanket and divertor) by the plasma (Roth *et al*., 2009). The particles are subject to conditions found in the vacuum vessel (VV) and may thus be radioactive (tritium and activation products (Di Pace *et al*., 2008)) or exhibit acute chemical toxicity like beryllium particles (Cortes *et al*., 2010; Rosanvallon *et al.,* 2008), or constitute, with air or water vapour, a potentially explosive mixture (Roth *et al*., 2009).

The mobility of these airborne particles and their containment in the event of an accident such as a LOVA have become, over time, a major topic for assessing the safety of ITER (Glor, 1985; Paci *et al*., 2005; Porfiri *et al*., 2006; Sharpe *et al*., 2002; 2006).

Several studies were conducted in order to understand the phenomenon of resuspension and to highlight the main

parameter which is the friction velocity (Garcia-Cascales *et al*., 2010; Gelain *et al*., 2015; Honda *et al*., 2000). These studies also allowed to characterize the competition between the airflow forces and the adhesive ones, especially depending on particle diameter, and to develop resuspension models such as the Rock'n Roll one (Reeks & Hall, 2001; Biasi *et al*., 2001).

Considering this latter, its application can be enforced in order to evaluate the risks caused by the particle resuspension in case of LOVA. For performing this step, the Rock'n'Roll model had to be implemented in a CFD code and precisely compared to experimental data.

This article proposes to develop the implementation of the Rock'n Roll model in a CFD code (ANSYS CFX) and to provide first result of its application to the case of a LOVA in a low pressure toroidal vessel.

However, even if the application proposed in this article is nuclear oriented, the issue of particle resuspension is present in numerous industrial situations in which powders are manipulated, can fall on the floor and can be resuspended by operator displacements. Hence, the present calculations could be extended to other industrial processes.

2. ROCK'N ROLL MODEL DESCRIPTION

The "Rock'n Roll" model, developed by Reeks & Hall (2001), on the basis of a so-called "RRH" model developed by Reeks *et al*. (1988), is founded on the assumption of a particle deposited on a rough surface which is resuspended by the airflow turbulence effect, such as shown in figure 1.

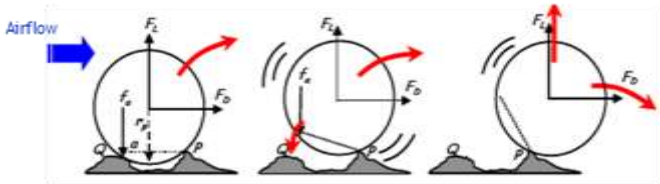

Figure 1 - scheme of understanding of the "Rock'n Roll" model

As observed on Figure 1, lift, drag and adhesive forces will create moments on the particle according to particle radius and the roughness scale of the floor.

This competition between adhesive and airflow moment forces can be expressed by the equation 1.

$$\frac{1}{2}F_L + \frac{r_p}{a}F_D > f_a \ , \qquad (1)$$

where F_L is the lift force, F_D is the drag force, f_a is the adhesive force, a is the distance between the two irregularities on which the particle rests and r_p the particle radius. According to experimental data analysed by Reeks & Hall (2001), the ratio r_p/a between the particle radius and the distance between two irregularities could be usually considered equal to 100.

This observation implies that the term including the lift force can, in most cases, be neglected, even if it is maintained in our case.

The drag and lift forces can be expressed by the following expressions:

$$\begin{aligned} F_D &= 8.01\rho\nu^2\left(d_p^+\right)^2 \quad \text{(O'Neill, 1968)}, \\ F_L &= 4.2\rho\nu^2\left(d_p^+\right)^{2.31} \quad \text{(Hall, 1988)}, \end{aligned} \qquad (2)$$

where ν is the fluid kinematic viscosity and d_p^+ is the non-dimensional particle diameter defined by:

$$d_p^+ = \frac{d_p . u^*}{\nu}, \qquad (3)$$

where u^* is the friction velocity and d_p is the particle diameter.

Taking into account these expressions, the balance of airflow forces required to mobilize a spherical particle deposited on a flat surface gives:

$$F = \frac{1}{2}F_L + \frac{r_p}{a}F_D = 2.1\rho\nu^2\left(d_p^+\right)^{2.31} + 801\rho\nu^2\left(d_p^+\right)^2. \qquad (4)$$

Adhesive forces cannot be simply expressed due to the floor roughness, but Reeks & Hall (2001) supposed that they are distributed according to a log-normal distribution given by:

$$\varphi(f_a') = \frac{1}{\sqrt{2\pi}}\frac{1}{f_a' \ln(\sigma_a')} e^{\left(-\frac{1}{2}\left(\frac{\ln\left(f_a'/\overline{f_a'}\right)}{\ln(\sigma_a')}\right)^2\right)}, \qquad (5)$$

where $f_a' = f_a/F_{JKR}$ represents the normalised adhesive force f_a(N) thanks to the JKR theoretical model. $\overline{f_a'}$ represents the geometric mean of normalised adhesive forces distribution and σ_a' the geometric standard deviation of the distribution.
The JKR model (Johnson *et al*., 1971) provides a theoretical adhesive force that takes into account particle deformation for an ideal system composed of a spherical particle on a smooth surface:

$$F_{JKR} = \frac{3}{4}\pi\gamma d_p, \qquad (6)$$

where γ represents the surface energy of the system particle/surface entering in interaction. Consequently f_a' could be view as a reduction factor from JKR force that allows to take into account surface and particle roughnesses.

For operational Rock'n Roll model calculation, Biasi *et al* (2001) proposed empirical correlations (eq. 7 and 8) as adhesion forces distribution parameter $\overline{f_a'}$ and $\overline{\sigma_a'}$, for model input.

These correlations were determined by fitting the Rock'n Roll model on numerous experimental data of particles resuspension for different kinds of particles and different deposit surfaces.

$$\overline{f_a'} = 0.016 - 0.0023\left(\frac{d_p}{2}\right)^{0.545}, \qquad (7)$$

$$\overline{\sigma_a'} = 1.8 - 0.136\left(\frac{d_p}{2}\right)^{1.4}. \qquad (8)$$

In equations 7 and 8, the particle diameter d_p is expressed in micrometer and the main data used to establish them correspond to particle-surface pairs with an adhesive surface energy approaching 0.56 J.m^{-2} and particle diameters between 0.1 µm and 30 µm.

As a synthesis of the model, it can be seen that it is mainly depending on the friction velocity u^*, the particle diameter

d_p and the adhesion surface energy γ, and the most of the existing models (Ziskind *et al.*, 1995) agree with this observation.

However, knowing the presence of the fluid density in the model and given the specific nature of the LOVA in terms of pressure change, it is necessary to take into account the variation of fluid density when calculating airflow forces affecting the resuspension and dispersion models.

The "Rock'n Roll" model aims at calculating the resuspension rate which needs to know the constant resuspension specific rate p for an adhesive force value f_a.

$$\begin{cases} p(f_a) = n_\theta \left(e^{\left(\frac{-(f_a-\bar{F})^2}{2\bar{f^2}}\right)} \Big/ \frac{1}{2}\left[1 + \mathrm{erf}\left(\frac{(f_a-\bar{F})}{\sqrt{2\bar{f^2}}}\right)\right]\right) \\ \qquad \text{if } f_a - \bar{F} \geq 0.75\sqrt{\bar{f^2}} \\ p(f_a) = n_\theta, \ \text{if } f_a - \bar{F} < 0.75\sqrt{\bar{f^2}} \end{cases}, \quad (9)$$

where n_θ is the surface-particle resonance frequency (s^{-1}), $\bar{F}$ and f are respectively the mean and fluctuating component of the instantaneous airflow force $F(t)$ (N); the expression of $\bar{F}$ is given at the equation 3, whereas the fluctuation f and the frequency n_θ can be calculated by the following equations, thanks to experimental measurements carried out by Hall (1988):

$$f = 0.2\,\bar{F}\,, \quad (10)$$

$$n_\theta = 0.00658\left(\frac{u^{*2}}{\nu}\right). \quad (11)$$

From the constant resuspension specific rate $p(f_a)$, the resuspension rate $\lambda(t)$, depending essentially on the particle diameter and the shear velocity, can be calculated according to airflow conditions: constant or variable.

2.1 Model for a constant shear velocity

Knowing the expressions of the constant resuspension specific rate p and the adhesive force distribution φ, the resuspension rate $\lambda(t)$ for constant airflow conditions, involving a constant shear velocity, can be calculated from the following expression proposed by Reeks & Hall (2001) in the "Rock'n'Roll" model:

$$\lambda(t) = \int_0^\infty \varphi(f_a')\,p(f_a')\,e^{-p(f_a')t}\,df_a' \ . \quad (12)$$

In order to obtain $p(f_a')$, f_a must be replaced by $(f_a'.F_{JKR})$ in the equation (9).

2.2 Model adaptation for a variable shear velocity

To take into account the transient configuration, it is necessary to discretize the time with a timestep Δt small enough for considering the shear velocity as constant. This adaptation was proposed by Choi et al. (2012) in a study on the particle resuspension during a footstep. The mean value of the resuspension rate $\bar{\lambda}(t)$ is thus calculated for the timestep Δt considered by the following expression:

$$\bar{\lambda}(t) = \frac{1}{\Delta t}\int_0^{\Delta t} \lambda(t)\,dt = \frac{1}{\Delta t}\int_0^\infty \varphi(f_a')\left(1 - e^{-p(f_a')\Delta t}\right)df_a'. \quad (13)$$

3. MODEL IMPLEMENTATION IN ANSYS CFX

The Rock'n Roll model was implemented in ANSYS CFX in order to take into account the resuspension phenomenon in aerosol transport and deposition calculations, allowing to assess the resuspended particle amount for issues related to dust explosion in nuclear reactors or of dust inhalation by operators.

For this implementation, the following particle transport equation is used:

$$\frac{\partial \rho Y_p}{\partial t} + \nabla.\left(\rho \mathbf{U} Y_p\right) = \nabla.\left(\left(\rho D + \frac{\mu_t}{Sc_t}\right)\nabla Y_p\right) + S_p, \quad (14)$$

where Y_p is the particle mass fraction, ρ is the carrier fluid density ($kg.m^{-3}$), $\mathbf{U}$ is the mean fluid velocity vector ($m.s^{-1}$), D is the particle diffusion coefficient ($m^2.s^{-1}$), μ_t is the eddy viscosity (Pa.s), Sc_t is the turbulent Schmidt number and S_p the global particle source term ($kg.m^{-3}.s^{-1}$).

The resuspension rate $\lambda(t)$ including Biasi's correlation for the adhesive forces distribution is thus implemented as a wall flux term, associated to the local particle surface concentration $C_s(t)$ ($kg.m^{-2}$):

$$S_{p,res} = \lambda(t) C_s(t). \quad (15)$$

As the particles are resuspended, the local particle surface concentration has to decrease over time by this way. Hence, a variable associated to the surface concentration has also been implemented in order to take into account this evolution.

$$\begin{cases} C_s(t+\Delta t) = C_s(t)(1 - \lambda(t)\Delta t), \text{if } u^* \text{ is constant} \\ C_s(t+\Delta t) = C_s(t)\left(1 - \bar{\lambda}(\Delta t)\Delta t\right), \text{if } u^* \text{ is variable} \end{cases}. \quad (16)$$

Both types of model, either for a constant shear velocity, or for a variable one, have thus been implemented in ANSYS CFX and their preliminary validation has been conducted thanks to experimental data acquired on experimental benches available at IRSN. Some comparisons between CFX calculations and experiments on particle resuspension for transient flow are presented in Gelain (2014).

It should be noticed that a specific model for the particle transport and deposition, developed and validated by IRSN (Nérisson, 2011), was also implemented in ANSYS CFX. The transport model is integrated to the transport equation (14), whereas the deposition model is implemented as a wall sink term $S_{p,dep}$ added to the resuspension flux term $S_{p,res}$.

4. APPLICATION TO THE CASE OF A LOVA IN A TOROIDAL GEOMETRY

4.1 CFD simulation description

To evaluate the resuspension of different particle sizes from the airflows generated during a LOVA, numerical simulations were performed using ANSYS CFX software, into which the resuspension model with a variable shear velocity was implemented.

The first step consists in representing the geometry of the torus with the duct that simulates the breach which is the source of the loss of vacuum.

For the vessel, a toroidal geometry is retained with a D-shaped section, the dimensions of which are given in Table 1.

Table 1– overall dimensions of the torus

(ITER-FEAT,2000)

Torus volume	1,300 m^3
Inside radius of torus	3.99 m
Outside radius of torus	8.53 m
Height of torus	9.62 m

To represent the breach, a circular duct with a diameter of 0.16 m and a length of 2 m is used [ITER-FEAT, 2000]. The duct (representative of the equatorial port) is located halfway up the torus and is initially closed at the torus wall. Figure 2 presents a sectional view of the shape of the torus with its dimensions.

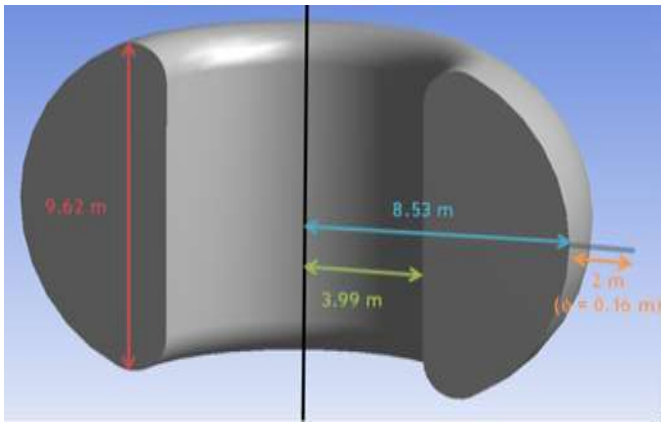

Figure 2 - geometry used for calculations

The mesh is presented in Figure 3.

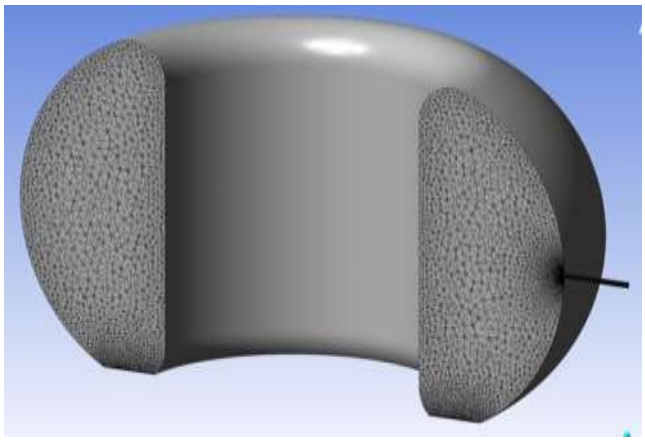

Figure 3 - geometry used for calculations

For the resuspension issues, the refinement close to the wall is important and may have consequences about the amount of resuspended particles, but currently, the resuspension model is not accuracy enough to calculate all the phenomena occurring at the vicinity of the wall and of the roughness. Hence, the aim of this study is not to validate the model or the modelling but to verify the model implementation relevance and the capabilities of this model to evaluate the resuspension in the case of low pressure. A more accurate validation will be conducted as soon as relevant experimental data will be available.

The dataset parameters for the calculations are given in Table 2. The k-ω SST turbulence model was chosen after a sensitivity study described by Gelain *et al.* (2015). This model remains a good compromise between accuracy and calculation time. The particle surface energy of adhesion is the tabulated value for tungsten (4.4 $J.m^{-2}$). This latter is different from the main value used by Biasi for determining his correlation (0.56 $J.m^{-2}$). Hence, the calculation is probably not conservative regarding resuspension.

The airflow parameters used for the calculations were set for a LOVA-type accident scenario as described by Xiao *et al.* (2010) and already used by Gelain *et al.* (2015). They are given in Table 2. It is reminded that the initial pressure in this calculation is about 800 Pa whereas, in ITER conditions, the pressure is about 10^{-7} Pa. The latter is too much low to ensure the validity of Navier-Stokes equation and 800 Pa is a good compromise between low pressure conditions and calculation robustness and convergence. Furthermore, what we want also to visualize with this calculation is this impact of lack of air on the resuspension and on the aerosols transport.

Table 2 – Parameters adopted for the modelling

Inlet pressure	10^5 Pa
Inlet air temperature	298 K
Initial torus pressure	800 Pa
Imposed torus wall temperature	673 K
Initial gas temperature	493 K
Particle density (tungsten)	19.3 $g.cm^{-3}$
Particle diameter d_p	2 – 5 – 10 µm (corresponding to 8.8 – 22 – 44 µm aerodynamic particle diameters)
Surface energy of adhesion JKR	4.4 $J.m^{-2}$
Turbulence models	k-ω SST
Time step	Adaptive from 10^{-6} second to 0.1 second
Duration	20 seconds

Before starting the resuspension calculation, the floor has to be seeded by a particle surface concentration. For that, a concentration source term was applied in the first cell of the mesh close to the floor.

During the calculation, the resuspension coefficient K_{res} and the resuspension rate λ_{res} were tracked in real time as well as the other usual variables such as the friction velocity, the particle mass fraction, the pressure or the floor surface concentration.

It can be noticed that the calculation was stopped at 20 s (for an inside pressure of around 12,000 Pa) because the friction velocities on the floor became too low to induce any particle resuspension.

In the next section, the simulation results are presented and discussed in terms of airflows, particle resuspension and dispersion.

4.2 CFD simulation results

- ***Airflows***

The particle resuspension is essentially driven by the airflows and more precisely by the friction velocity. Hence, Figure 4 presents the time evolution of the friction velocity on the bottom where the particles are dropped off. As seen on this figure, the maximal friction velocity reaches around 8 m/s for a mean velocity of around 4 m/s.

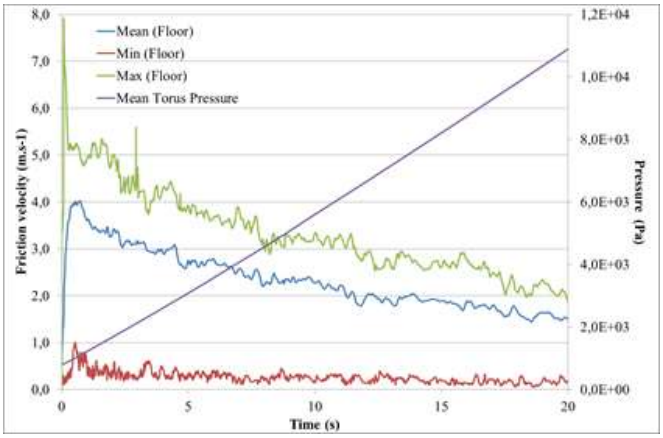

Figure 4 – friction velocity on the floor and pressure inside the torus

Figure 5 shows the friction velocity fields on the floor at different times that enables to visualize its distribution.

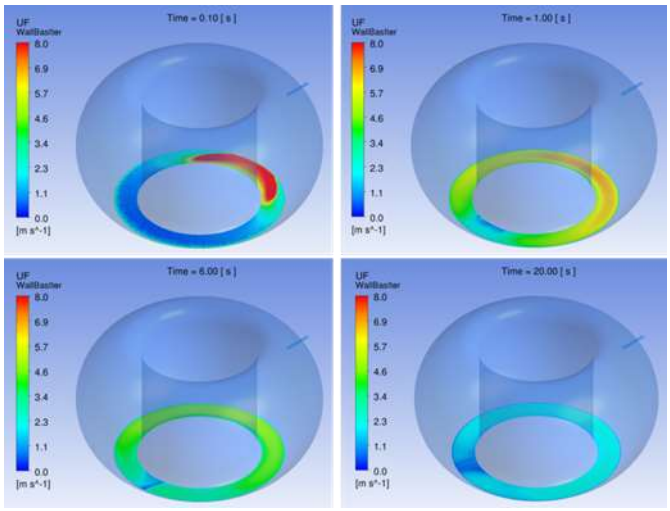

Figure 5 – friction velocity fields on the floor at 0.1 s, 1 s, 6 s and 20 s

Finally, Figure 6 shows the airflow streamlines inside the torus.

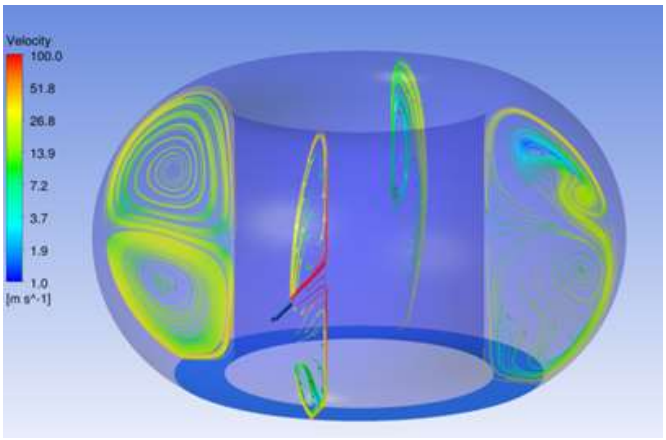

Figure 6 - airflow streamlines inside the torus (t = 1s)

The geometry and the high velocities induce vortices which will entrain the particles along the torus walls and disperse them inside the torus. The observation of these vortices is very important to understand how the particles are dispersed as shown in the next paragraph.

- ***Particle resuspension and dispersion***

As an illustration of the resuspension phenomenon during the calculation, Figure 7 shows the evolution of an isosurface of the particle normalized mass fraction (mass fraction divided by the maximal mass fraction) during the pressurization.

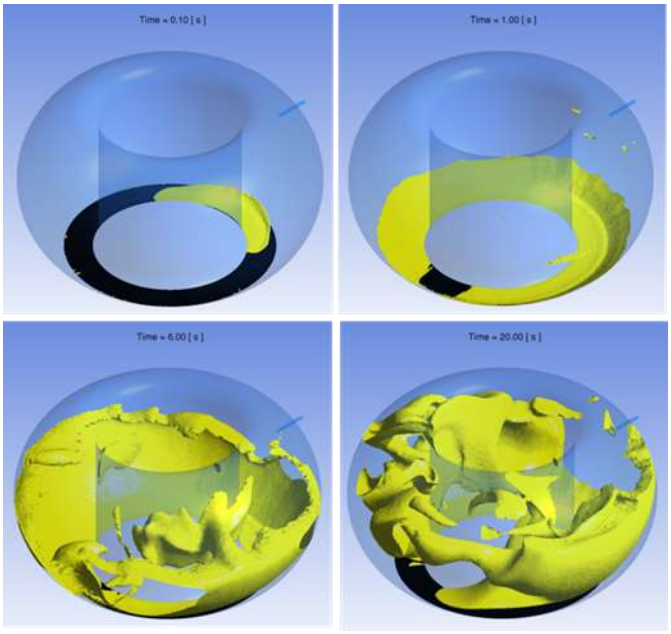

Figure 7 – time evolution of the isosurface at 0.001 of the resuspended normalized particle mass fraction at 0.1 s, 1 s, 6 s and 20 s (d_p = 10 µm diameter)

At the beginning, for the time 0.1 s, it can be seen that the resuspension of the particles is in good agreement with the friction velocity field of Figure 5. Indeed, as previously mentioned, the friction velocity is the main parameter of the resuspension where the drag force on particles has to overcome the adhesive forces, which mainly depend on the

particle diameter. So there is a threshold from which the resuspension happens which explains that just a little area of the floor exhibits resuspension. At the time 1 s, the friction velocity is higher on a larger area of the floor; hence, the resuspension is more extended on this area, in agreement with the friction velocity field of Figure 5. For the following times 6 s and 20 s, the friction velocities on the floor are lower; so, the resuspension too, and what is observed in Figure 7 is mainly the particle dispersion in the torus. The particles are carried along the wall, following the airflow streamlines as shown on Figure 6.

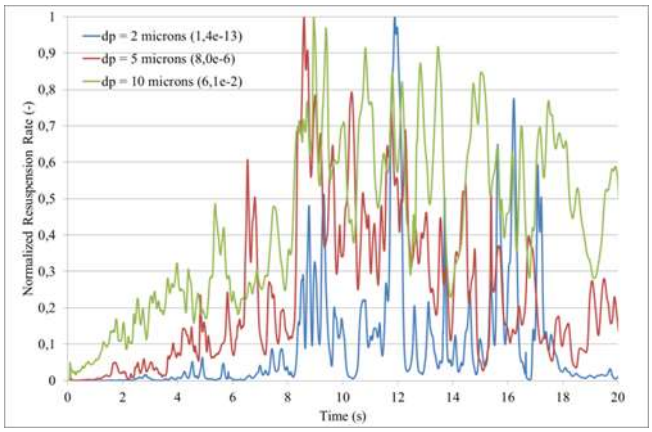

Figure 8 – resuspension rate time evolution for the three diameters studied

Figure 8 illustrates the time evolution of the resuspension rate normalized by the maximum value during 20 s, for the three studied diameters. The maximum values are indicated in the figure legend.

As indicated in the legend of Figure 8, the resuspension rates are very different according to the diameter. Around eleven decades are observed between resuspension rate for the 2 µm aerosol and that for 10 µm .

Otherwise, the resuspension kinetics is also slightly different; for the 2 µm aerosol, the latter begins to be significantly resuspended from 8 s, then the resuspension stays constant up to 18 s, before decreasing. In contrast, for the 5 and 10 µm aerosol, the resuspension occurs almost at the beginning of the pressurization and is still on at 20 s.

These observations can be confirmed by the evolution of the resuspension coefficients in Figure 9. This latter presents the resuspension coefficient time evolution (solid lines), corresponding to the floor source term, and the "in suspension" coefficient time evolution (dash lines), corresponding to the particles effectively in suspension in the torus at the given time. The difference between both is the deposition on the torus wall. On the secondary axis is presented the time evolution of the pressure in the torus.

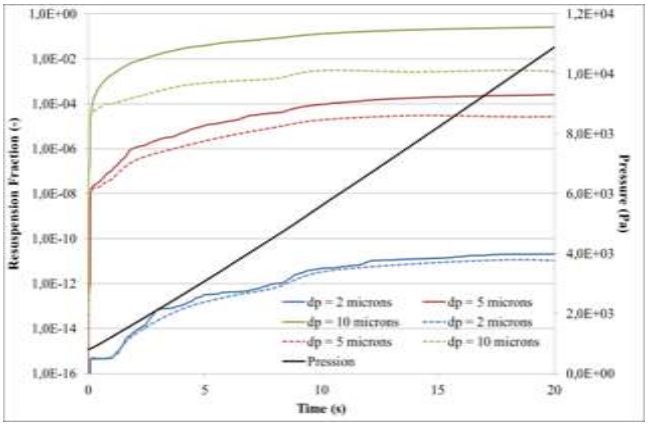

Figure 9 – resuspension fraction time evolution

Figure 9 shows that the biggest particles are the most resuspended but also the most deposited. However, it can be observed that for the 10 µm aerosol, the total particle resuspension coefficient can reach around 25 % for the calculation conditions.

5. CONCLUSIONS

This article presents the implementation of the Rock'n'Roll model in a CFD code (ANSYS CFX) and an application to the case of a LOVA in toroidal geometry.

In a first part, the Rock'n'Roll model integrating the adhesive force distribution of Biasi *et al.* (2001) was described, before detailing the model implementation in ANSYS CFX, performed by the way of a source term of resuspension in the particle transport equation. The model can be used with a constant or a variable friction velocity according to the model formulation.

Then, an application of the model to a LOVA case in a toroidal geometry was presented. This type of simulation is slightly complex due to the lower pressure close to the vacuum which evolves with the air ingress.

These simulations carried out for 2, 5 and 10 µm dust corresponding to 8.8, 22 and 44 µm aerodynamic diameters showed a relevant kinetics of resuspension according to the friction velocity fields on the floor where the particles are dropped off and to the airflows which entrain the particle into the torus. The results are also in agreement with the particle resuspension physics showing a larger resuspension amount for the 10 µm aerosol than for the 2 µm one with a difference of many decades between both.

This article demonstrates thus the feasibility of particle resuspension CFD simulations with the Rock'n Roll model, allowing to evaluate quantitatively the particle resuspension. However, this model with the Biasi's formulation takes into account a one layer particle surface deposition which may not be the reality in most cases. So a prospect for improving these simulations could be to implement a multi-layer particle surface deposition or to better take into account the adhesive forces by the way of recent studies which could be applied to this case. Finally, recent numerical and experimental results showed the influence of the particle polydispersity on their resuspension.

NOMENCLATURE

Latin letters

a	distance between two floor irregularities (m)
C_s	floor surface concentration (kg.m^{-2})
D	diffusion coefficient (m^2.s^{-1})
d_p	particle diameter (m)
F, f	force (N)
p	constant resuspension specific rate (s^{-1})
r_p	particle radius (m)
S_p	particle source flux (kg.m^{-2}.s^{-1})
Sc_t	turbulent Schmidt number
t	time (s)
u^*	friction velocity (m.s^{-1})
U	velocity (m.s^{-1})
V_d	deposition velocity (m.s^{-1})
y^+	non-dimensional wall distance
Y_p	particle mass fraction

Greek letters

λ	resuspension rate (s^{-1})
ρ	density (kg.m^{-3})
ν	kinematic viscosity (m^2.s^{-1})
σ	geometric standard deviation
μ_t	eddy viscosity (Pa.s)

REFERENCES

Biasi L., De los Reyes A., Reeks M. W., and De Santi G. F. (2001). Use of a simple model for the interpretation of experimental data on particle resuspension in turbulent flows. Journal of Aerosol Science 32 (10), 1175–1200.

Choi J-I., Edwards J.R., Rosati J.A. and Eisner A.D. (2012). Large eddy simulation of particle resuspension during a footstep. Aerosol Science and Technology 46 (7), 767-780.

Cortes P., Taylor N., Rosanvallon S., Rodriguez-Rodrigo L., Elbez-Uzan J., Iseli M. and Ciattaglia S. (2010). Optimization at the design phase of the potential impact of ITER on workers, the public and the environment. Fusion Engineering and Design 85, 2263-2267.

Di Pace L., Letellier E., Maubert H., Patel B. and Raskob W. (2008). Biological hazard issues from potential releases of tritiated dust from ITER. Fusion Engineering and Design 83, 1729-1732.

García-Cascales J.R., Vera-García F., Zueco-Jordán J., Bentaib A., Meynet N., Vendel J., Perrault D. (2010). Development of a IRSN code for dust mobilisation problems in ITER, Fusion Engineering and Design 85, 2274–2281.

Gelain T., Rondeau A., Peillon S., Sabroux J.C., Gensdarmes F. (2015). CFD modelling of the wall friction velocity field in the ITER tokamak resulting from airflow during loss of vacuum accident-Consequences for particle resuspension. Fusion Engineering and Design 100, 87-99.

Gelain T., Gensdarmes F., Peillon S., Ricciardi L. (2020). CFD modelling of particle resuspension in a toroidal geometry resulting from airflows during a loss of vacuum accident (LOVA). Fusion Engineering and Design 151.

Glor M. (1985). Hazards due to electrostatic charging of powders. Journal of Electrostatics 16, 175-191.

Hall, D. (1988). Measurements of the mean lift force on a particle near a boundary layer in turbulent flow. Journal of Fluid Mechanics 187, 451.

Honda T., Bartels H.-W., Merrill B., Inabe T., Petti D., Moore R., Okazaki T. (2000). Analyses of loss of vacuum accident (LOVA) in ITER. Fusion Engineering and Design 47, 361-375.

ITER-FEAT - Outline Design Report (2000). ITER Meeting, Tokyo. www.fire.pppl.gov/ODR_IC_final.pdf.

Johnson K.L., Kendall K. and Roberts A.D. (1971). Surface energy and the contact of elastic solids. The Royal Society 324, 301-313.

Nerisson, P., Simonin, O., Ricciardi, L., Douce, A., Fazileabasse, J. (2011). Improved CFD transport and boundary conditions models for low-inertia particles. Computers & Fluids 40 (1), 79-91.

Paci S., Forgione N., Parozzi F., Porfiri M.T. (2005). Bases for dust mobilization modelling in the light of STARDUST experiments. Nuclear Engineering and Design 235, 1129-1138.

Porfiri, M.T., Forgione, N., Paci, S., Rufoloni, A (2006). Dust mobilization experiments in the context of the fusion plants—STARDUST facility, Fusion Eng. Des. 81, 1353–1358.

Reeks M.W., Reed J., Hall D. (1988). On the resuspension of small particles by a turbulent flow. Journal of Physics D: Applied Physics 21, 574-589

Reeks M.W., Hall D. (2001). Kinetic models for particle resuspension in turbulent flows: theory and measurement. Journal of Aerosol Science 31 (1), 1-31

Rosanvallon S., Grisolia C., Counsell G., Hong S.H., Onofri F., Worms J., Winter J., Annaratone B.M., Maddaluno G. and Gasior P. (2008). Dust control in tokamak environment. Fusion Engineering and Design 83, 1701-1705.

Roth J., Tsitrone E., Loarte A., Loarer T., Counsell G., Neu R. Philipps V., Brezinsek S., Lehnen M., Coad P., Grisolia C., Schmid K., Krieger K., Kallenbach A., Lipschultz B., Doerner R., Causey R., Alimov V., Shu W., Ogorodnikova O., Kirschner A., Federici G. and Kukushkin A. (2009). Recent analysis of key plasma wall interactions issues for ITER. Journal of Nuclear Materials 390, 1-9.

Sharpe J.P., Petti D.A., Bartels H.-W (2002). A review of dust in fusion devices: Implications for safety and operational performance. Fusion Engineering and Design 63-64, 153-163.

Sharpe J.P., Humrickhouse P.W. (2006). Dust mobilization studies in the TDMX facility. Fusion Engineering and Design 81, 1409-1415.

Van Dorsselaere J.P., Perrault D., Barrachin M., Bentaib A., Gensdarmes F., Haeck W., Pouvreau S., Salat E., Seropian C., Vendel J. (2012). Progress of IRSN R&D on ITER Safety Assessment. Journal of Fusion Energy 31, 405–410.

Xiao, J., Travis, J.R., Breitung, W., Jordan, T. (2010).

Numerical analysis of hydrogen riskmitigation measures for support of ITER licencing, Fusion Eng. Des. 85, 205–214.

Ziskind G., Fichman M. and Gutfinger C. (1995). Resuspension of particulates from surfaces to turbulent flows - review and analysis. Journal of Aerosol Science 26, 613-644.